Charge Mobility and Recombination Mechanisms in Tellurium van der Waals Solid

Bhaskar, Prashant; Achtstein, Alexander W.; Vermeulen, Martien J.W.; Siebbeles, Laurens D.A.

DOI
10.1021/acs.jpcc.8b09665

Publication date
2019

Document Version
Final published version

Published in
Journal of Physical Chemistry C

THE JOURNAL OF PHYSICAL CHEMISTRY C

Article

Cite This: J. Phys. Chem. C 2019, 123, 841−847

pubs.acs.org/JPCC

Charge Mobility and Recombination Mechanisms in Tellurium van der Waals Solid

Prashant Bhaskar,* Alexander W. Achtstein,† Martien J. W. Vermeulen, and Laurens D. A. Siebbeles*

Optoelectronic Materials Section, Department of Chemical Engineering, Delft University of Technology, Van der Maasweg 9, 2629 HZ Delft, The Netherlands

ABSTRACT: Trigonal tellurium is a small band gap elemental semiconductor consisting of van der Waals bound one-dimensional helical chains of tellurium atoms. We study the temperature dependence of the charge carrier mobility and recombination pathways in bulk tellurium. Electrons and holes are generated by irradiation of the sample with 3 MeV electrons and detected by time-resolved microwave conductivity measurements. A theoretical model is used to explain the experimental observations for different charge densities and temperatures. Our analysis reveals a high room temperature mobility of 190 ± 20 $cm^2\ V^{-1}\ s^{-1}$. The mobility is thermally deactivated, suggesting a band-like transport mechanism. According to our analysis, the charges predominantly recombine via radiative recombination with a radiative yield close to 98%, even at room temperature. The remaining charges recombine by either trap-assisted (Shockley−Read−Hall) recombination or undergo trapping to deep traps. The high mobility, near-unity radiative yield, and possibility of large-scale production of atomic wires by liquid exfoliation make Te of high potential for next-generation nanoelectronic and optoelectronic applications, including far-infrared detectors and lasers.

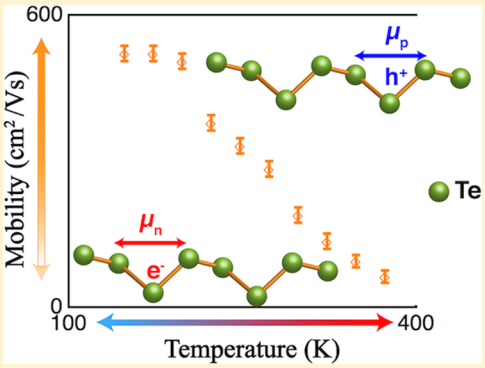

INTRODUCTION

Extensive studies on fundamental properties of two-dimensional (2D) van der Waals materials have revealed new possibilities for the development of next-generation optoelectronic devices.[1−8] Two-dimensional materials, where layers of strongly bound atoms are weakly held together by van der Waals forces, exhibit the possibility of separating the layers via exfoliation techniques, allowing one to engineer their electronic and optical properties. Similar to 2D materials, in one-dimensional (1D) materials, covalently bound chains of atoms are held together by weak van der Waals forces in the two perpendicular directions. Such 1D materials also have interesting promising applications in nanoelectronics. Two such impeccable 1D systems are trigonal selenium (Se) and tellurium (Te), which have crystal structures that consist of helical chains of atoms. These materials exhibit potential for various applications due to their stability in air. As proposed for Se,[9] exfoliation of bulk Te to obtain 1D atomic chains of Te has been demonstrated recently.[10] However, Te is different from Se because of strong interchain electronic coupling in the bulk, thus being a quasi-1D system.[11] In addition, the 0.33 eV band gap of Te[12,13] is much lower than the 1.9 eV band gap of Se.[13]

As a 1D van der Waals material, Te has been widely studied for its electronic structure,[13−16] optical properties,[12,13,17] Hall conductivity, and extrinsic mobility in p-type Te.[18−21] Very recently, it gained attention due to its high thermoelectric figure of merit.[22,23] The aforementioned studies on conductivity and mobility have mostly been performed at low temperatures (∼77 K),[20] with externally doped samples and using contact measurements.[20,24] Therefore, it is of great interest to study its intrinsic optoelectronic properties without external doping and at temperatures close to ambience.

In the present investigation, we provide insights into temperature-dependent intrinsic charge carrier mobility and decay mechanisms in trigonal Te with varying charge carrier density, building up on our earlier results on other van der Waals materials.[9,25] Quantitative analysis of our experimental observations reveals the characteristics of charge carrier mobility and recombination in the quasi-1D atomic chains of Te in bulk, laying the basis for further investigations of exfoliated Te. The high mobility and near-unity quantum yield (QY) make Te of interest for nanoelectronics and optoelectronics. These properties and the low band gap make Te a promising material for use in far-infrared detectors. The appreciably high mobility and quantum yield result in low device resistance and $1/f$ noise, which are essential to realize a high S/N ratio.[26]

EXPERIMENTAL METHODS

Te pellets with purity 99.999% were procured from Sigma-Aldrich (now MERCK) and used as received without any

Received: October 3, 2018
Revised: November 23, 2018
Published: December 12, 2018

DOI: 10.1021/acs.jpcc.8b09665
J. Phys. Chem. C 2019, 123, 841−847

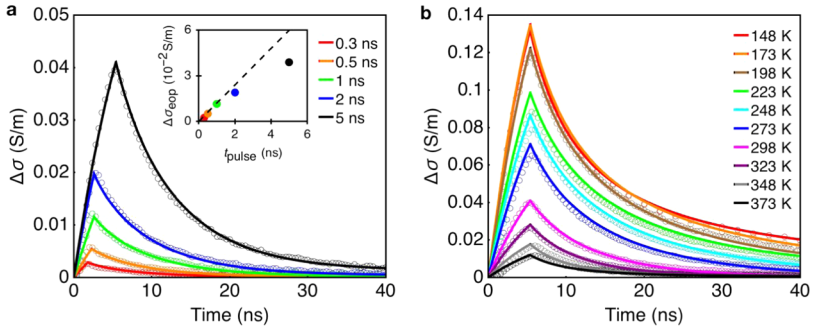

Figure 1. Transient microwave conductivity due to excess charge carriers in tellurium at room temperature (298 K) for various durations of the 3 MeV electron pulse (curves with markers) and as obtained from theoretical modeling (solid curves) (a) and for various temperatures, as labeled (b). The inset shows the conductivity at the end of the electron pulse $\Delta\sigma_{eop}$, as a function of pulse duration t_{pulse}.

further treatment. Te pellets were finely powdered using a mortar and pestle for studying contactless microwave conductivity at various temperatures and at various densities of excess electrons and holes. The microwave conductivity studies were performed at frequencies in the range of the K_a band (27−38 GHz), similar to our previous studies.[9,25] Uniform densities of excess electrons and holes were generated by irradiation with 3 MeV electron pulses from a van de Graaff accelerator, along with Bremsstrahlung irradiation, which was produced by retarding the electron pulses by a 2 mm lead (Pb) sheet. The high-energy Bremsstrahlung photons generate electron−hole pairs along their paths through the sample. Successive irradiation of the sample had no effect on the transient conductivity, implying the absence of radiation-induced damage.

The powdered Te sample was filled into a polyether-etherketone (PEEK) sample holder with a groove of 1 mm along the direction of high-energy irradiation. In this sample holder, the sample height along the direction of electron irradiation is 1 mm, whereas the sample holder size is close to 3.5 mm. Such a sample holder was designed to avoid nonuniform generation of charges, as would have occurred because of stopping of high-energy electrons within the sample, discussed next. As tellurium is a heavy material, with atomic number Z = 52, density ρ_{Te} = 6.2 g cm^{-3}, and M_{Te} = 127.60 g mol^{-1}, it exhibits a comparatively higher stopping power ($S(E) = -dE/dx$) for the 3 MeV electrons, as compared to materials we studied previously.[9,25] A higher stopping power leads to lower average penetration depth (Δx) for the 3 MeV electrons in the sample, which leads to a nonuniform distribution of charges inside the sample. To avoid a nonuniform charge density, the sample height was reduced so that the high-energy electrons could pass through the sample, generating a close to uniform distribution. The stopping power and average penetration depth values were calculated using eqs 1 and 2, respectively, which were obtained by simplifying Bethe's expression for the collisional mass stopping power (also known as linear energy transfer) for high-energy electrons.[27−30]

$$(S)_{Te} = \left(\frac{S}{\rho}\right)_{H_2O} \frac{18}{10}\rho_{Te}\frac{Z_{Te}}{M_{Te}} \quad (1)$$

$$\Delta x = \int_0^{E_0} \frac{1}{S(E)}dE \quad (2)$$

In eqs 1 and 2, ρ is the mass density,[31] Z is the atomic number, M is the elemental or molecular weight, and E_0 is the 3 MeV energy of incident electrons. Equations 1 and 2 yield an average penetration depth of 3.5 mm. Because this significantly exceeds the sample width of 1 mm, a uniform density of electrons and holes is produced upon irradiation.

The stacked dual-layered structure consisting of Te and PEEK sample holder results in a heterogeneity of the sample along the direction of irradiation. In such a case for studying microwave absorption, the effective dielectric constant of a heterogeneous sample can be estimated by considering the Maxwell−Wagner effect, which is described by[32−34]

$$\varepsilon_* = \varepsilon_*' - j\varepsilon_*'' = d\left[\sum_i \frac{d_i}{\varepsilon_i' - j\varepsilon_i''}\right]^{-1} \quad (3)$$

In the above equation, d is the total height of the layered sample, d_i is the height of the ith layer, ε_i' (ε_i'') is the real (imaginary) part of the permittivity of the ith layer, ε_* corresponds to the effective dielectric constant and $j^2 = -1$. This effect introduces a sensitivity factor B, which is used to obtain the conductivity in absolute values (discussed below).

Because of very high conductivity signals of Te, nearly saturating the electronic regime of the experimental setup, even for a short electron pulse duration of 500 ps, the radiation dose was reduced by using a 2 mm Pb plate placed at the top of the experimental cell containing the sample. The introduction of the Pb plate resulted in a reduction of the irradiation dose by 70 times because of partial stopping of 3 MeV electrons in the plate and production of Bremsstrahlung. The reduction factor was deduced from a test experiment of Te using 300 ps electron pulse with and without using a Pb plate, for which the conductivity signal was well within the saturation range. The final dose on the sample is a result of slowed down electrons as well as Bremsstrahlung. The incident high-energy electrons together with the Bremsstrahlung resulted in the formation of uniformly distributed electrons and holes in the sample with number density G per unit time. G is given by the ratio of the known energy-transfer rate (radiation dose per unit time) from the irradiation and the energy required for the formation of an electron−hole pair.

The radiation dose in Te, D_{Te}, was obtained from a reference measurement on benzene (Bz), which was found to be 530 J m^{-3} nC^{-1},[35] according to $D_{Te} = D_{Bz}(N_{e,Te}\rho_{Te}M_{Bz}/N_{e,Bz}\rho_{Bz}M_{Te})$, followed by a reduction of 70 times due to the Pb sheet, where N, ρ, and M are the number of the electrons per atom/molecule, mass density, and atomic/molecular mass for Te or

DOI: 10.1021/acs.jpcc.8b09665
J. Phys. Chem. C 2019, 123, 841−847

Bz, respectively. The electron−hole pair formation energy, E_p, was estimated from the empirical relation provided by Alig et al.,[36] which is given by $E_p = 2.73E_g + b$, where $b = 0.5$ eV and $E_g = 0.33$ eV,[13] the band gap of Te. The density of generated electron−hole pairs is given by the ratio D_{Te}/E_p, and the generation rate of electron−hole pairs during the 3 MeV electron pulse with a rectangular shape during time and duration t_{pulse} is equal to $G = D_{Te}/(E_p t_{pulse})$.

The transient conductivity, $\Delta\sigma(t)$, due to excess charge carriers is obtained from the measured change of microwave power reflected from the cell, according to $\Delta P(t)/P = -AB\Delta\sigma(t)$, where A and B are sensitivity factors. Whereas A depends on the cell dimensions and dielectric constant of the sample, B takes into account the heterogeneity of the sample by introducing a factor corresponding to an effective dielectric constant of the sample, as described previously.[34,37]

RESULTS AND DISCUSSION

Transient Microwave Conductivity Due to Excess Electrons and Holes. Figure 1 shows the transient microwave conductivity traces obtained for various pulse durations and temperatures as indicated. The traces with markers are the experimental results, whereas the solid traces overlaid on them are obtained upon theoretical modeling as discussed below.

The transient conductivity increases during the 3 MeV electron pulse due to generation of excess mobile electrons and holes in the sample. Also, the end-of-the-pulse conductivities ($\Delta\sigma_{eop}$) increase as the pulse duration becomes longer from 0.3 ns through 5 ns (see in Figure 1a) due to a higher charge carrier density for a longer pulse. The inset in Figure 1a shows $\Delta\sigma_{eop}$ as a function of pulse duration (t_{pulse}). The sublinear increase in $\Delta\sigma_{eop}$ with t_{pulse} is due to higher-order recombination of charges in addition to the first-order trapping. Subsequently, the electrons and holes decay by recombination or trapping.

Theoretical Model of Charge Carrier Generation and Decay Dynamics. The transient microwave conductivity is given by $\Delta\sigma(t) = e[\mu_{n_1}\Delta n_1(t) + \mu_{n_2}\Delta n_2(t)]$, where μ_{n_1} and μ_{n_2} are mobilities for charge particles of type n_1 and n_2. Because we cannot distinguish electrons from holes, charges of type n_1 and n_2 correspond to electrons and holes, respectively, or vice versa. The excess charge densities are equal to $\Delta n_1(t)$ and $\Delta n_2(t)$ and e is the elementary charge. We describe the conductivity signals theoretically by taking into account the generation of excess electrons and holes with a generation rate $G = (3.1 \pm 0.4) \times 10^{14}$ cm^{-3} ns^{-1} during the 3 MeV electron pulse, followed by recombination with each other or with the intrinsic electrons and holes that are already present in equal densities $n_i(T)$, at temperature T, or by trapping at defects. The thermal generation and recombination at a given temperature results in significant equilibrium densities of electrons and holes due to the low Te band gap of $E_g = 0.33$ eV.[13]

Charge mobilities and decay kinetics were obtained by fitting a theoretical model to the measured conductivity traces, where excess electron and hole transient densities are described according to the coupled differential equations given by

$$\frac{d\Delta n_1(t)}{dt} = G_{pulse}\phi_{n_1} - \frac{k_{n_1}^{SRH}k_{n_2}^{SRH}[n_1(t)n_2(t) - n_i^2]}{(k_{n_1}^{SRH}n_1(t) + k_{n_2}^{SRH}n_2(t))} - \frac{\beta_{n_1}(k_{n_1}t)^{\beta_{n_1}}}{t}n_1(t) - k_r[n_1(t)n_2(t) - n_i^2] \quad (4)$$

$$\frac{d\Delta n_2(t)}{dt} = G_{pulse}\phi_{n_2} - \frac{k_{n_1}^{SRH}k_{n_2}^{SRH}[n_1(t)n_2(t) - n_i^2]}{(k_{n_1}^{SRH}n_1(t) + k_{n_2}^{SRH}n_2(t))} - \frac{\beta_{n_2}(k_{n_2}t)^{\beta_{n_2}}}{t}n_2(t) - k_r[n_1(t)n_2(t) - n_i^2] \quad (5)$$

The total electron or hole density is $n_1(t) = n_i + \Delta n_1(t)$ (and $n_2(t) = n_i + \Delta n_2(t)$), where $\Delta n_1(t)$ (and $\Delta n_2(t)$) is the density of excess electrons or holes produced by the incident high-energy irradiation. Note, that the initial excess densities are equal, i.e., $\Delta n_1(t = 0) = \Delta n_2(t = 0)$. Further, the first term describes the generation of electrons and holes with a rate $G_{pulse} = G[\Theta(t) - \Theta(t - t_{pulse})]$, where Θ is the Heaviside function making the expression nonzero only during the high-energy irradiating pulse with duration t_{pulse}. Furthermore, ϕ_{n_1} and ϕ_{n_2} denote the fraction of initially generated charges surviving from direct trapping or geminate electron−hole recombination during the 3 MeV electron pulse. Terms containing the factor n_i^2 take into account the generation of electron−hole pairs by deviation from the thermodynamic equilibrium carrier density n_i through absorption of blackbody radiation, thermal excitation, or impact ionization by sufficiently energetic intrinsic thermally excited charge carriers.[38] The intrinsic density of charge carriers is given by $n_i = \sqrt{\left(\frac{m_e^* m_h^* k_B^2 T^2}{\pi^2\hbar^4}\right)^{3/2}} e^{-E_g/2k_BT}$ for a three-dimensional (3D) semiconductor,[39] with m_e^* and m_h^* being the effective masses of electrons and holes taken from previous reports, respectively.[12,15] Furthermore, k_B denotes the Boltzmann constant, T the temperature, and $\hbar$ the reduced Planck constant. Note, that Liu et al.[11] reported that the interchain electronic coupling of Te atomic wires is comparable to the intrachain electronic coupling. This causes Te to behave almost like an isotropic 3D system rather than a 1D system such as Se, so that the use of the 3D intrinsic carrier density above is substantiated.

The second terms in eqs 4 and 5 take into account trapping and subsequent nonradiative electron−hole recombination according to the Shockley−Read−Hall (SRH) model,[38] neglecting defect parameters (the densities of electrons and holes in case the Fermi energy coincides with the trap level[40]). The parameters $k_{n_1}^{SRH}$ and $k_{n_2}^{SRH}$ denote the trapping rate constants for SRH recombination. In an ideal case, they are proportional to the trap density and electron- and hole-capture coefficients, which depend upon the thermal velocity of the charges.[41] However, the temperature dependence of trapping rate constants may, nevertheless, deviate from the ideal case, e.g., when trapping processes are thermally activated. The third terms in eqs 4 and 5 represent charge trapping with the characteristic rate k_{n_1} (and k_{n_2}), which by themselves yield a stretched-exponential (quasi-exponential or Kohlrausch)[42] decay given by $n(t) = n(t = 0)\exp[(-kt)^{\beta}]$,[43,44] where β is a parameter that characterizes dispersive charge diffusion in an exponential energy landscape. For an exponential distribution

DOI: 10.1021/acs.jpcc.8b09665
J. Phys. Chem. C 2019, 123, 841−847

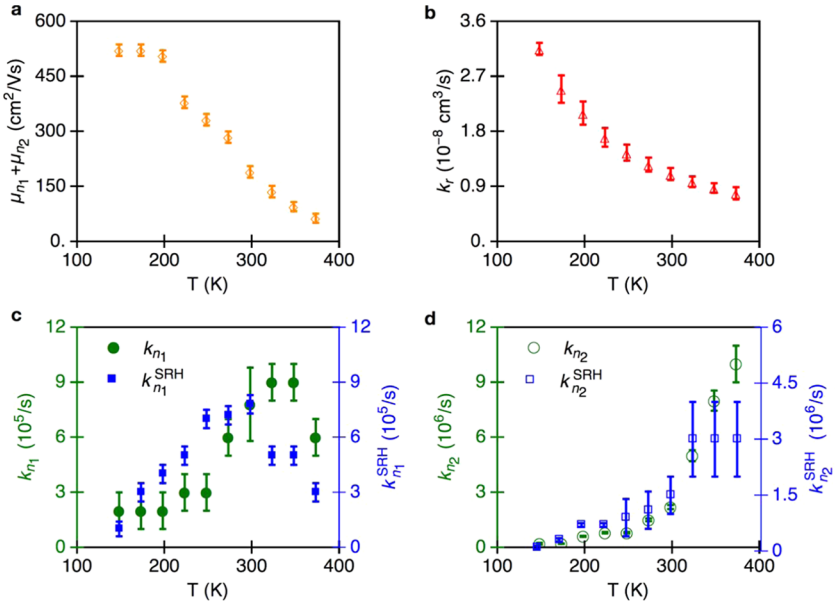

Figure 2. Temperature dependence of fitting parameters obtained from the theoretical model: (a) the combined mobility of electrons and holes, (b) radiative recombination rate constant k_r, (c) and (d) SRH recombination rate constant and decay rate for stretched-exponential trapping for electrons or holes (n_1) and their respective counter charges (n_2).

of trap site energies of width k_BT_0, the β parameter is given by $\beta = T/T_0$.[43,45−47] The fourth terms in eqs 4 and 5 account for radiative recombination of an electron−hole pair with rate coefficient $k_r = pE_g^2/(k_BT)^{3/2}$, with p as a constant independent of temperature.[25,41,48] The decrease of k_r with temperature is understood in terms of the decreasing likelihood of matching equal but opposite momenta of free carriers, imposed by momentum conservation during recombination, as the average thermal energy and hence Fermi vector increases with temperature.[48]

Temperature-Dependent Electron and Hole Mobility and Decay Rate Coefficients. Figure 1 shows that the theoretical model, given by eqs 4 and 5, reproduces the measured transient conductivities. The fitted parameters, combined electron and hole mobility ($\mu_{n_1} + \mu_{n_2}$), band-to-band radiative recombination (k_r), Shockley−Read−Hall rate constants ($k_{n_1}^{SRH}$ and $k_{n_2}^{SRH}$), and characteristic rate constants for stretched exponential decay of charges (k_{n_1} and k_{n_2}) are shown in Figure 2 as a function of temperature. The trapping rates for electrons and holes cannot be distinguished, as they are interchangeable. In our previous work on Se, electrons and holes could be distinguished because it was known from literature that electrons are trapped faster than holes.[9,49] Such information is not available for Te and consequently we cannot distinguish electrons and holes. Hence, the charge carrier densities and related rates and mobilities are denoted as n_1 for one type of charge and n_2 for the counter charge. As mentioned earlier, the numerical fits were found to reproduce the experimental results only for the calculated intrinsic density valid for a three-dimensional system and not for a one-dimensional system, in agreement with the finding of Liu et al.[11] Additionally, the numerical fits could only reproduce the experimental data by taking the values for the initial yield of charges (ϕ in eqs 4 and 5) equal to unity. This implies that the initially generated charges do not undergo geminate recombination to form excitons, as could be expected because the exciton binding energy in Te is only 1.2 meV.[13] Furthermore, the charges are generated far apart in the sample, larger than the critical escape radius determined by the thermal energy.

The mobility obtained at room temperature is 190 ± 20 cm^2 V^{-1} s^{-1}. This value is somewhat lower than the values near 700 cm^2 V^{-1} s^{-1} reported for thin layers of 1D and 2D Te nanostructures in field-effect transistors (FETs).[24,50] The latter values can be higher than ours due to enhancement of the mobility for thinner samples[50] and/or due to the high charge density in field-effect transistor (FET) measurements resulting in filling of trap states. The high mobility in Te may be in part due to the absence of polar optical phonon scattering, which significantly limits the mobility in compound 2D semiconductors.[51] Figure 2a depicts that the combined electron and hole mobility decreases with temperature, which is typical for band-like transport. This can be because of the combined effect of various types of electron−phonon scattering processes. Classically, ionized impurity scattering of charges generally occurs because of elastic scattering of charges with ionized shallow-donor impurities in a semiconductor. Because of this scattering, the mobility is expected to increase with $T^{3/2}$ at low temperature.[41] Ionized impurity scattering leads to increase in mobility with temperature, which can be a reason for the initial flatness in the mobility trend up to 200 K together with another process decreasing the mobility with temperature. Above 200 K, the mobility decreases because of electron−phonon scattering. The observed decrease in the mobility with temperature in Te is in line with the trends in previous reports.[20,23]

Figure 2b shows the temperature dependence of the second-order band-to-band radiative recombination rate constant (k_r), which decreases with temperature, as expected from theory (see Theoretical Model of Charge Carrier Generation and Decay Dynamics section). The numerical fits to the experimental data in Figure 1 yield a room temperature value of k_r equal to $(1.1 \pm 0.1) \times 10^{-8}$ cm^3 s^{-1}. In the case of diffusion-limited radiative recombination, the rate constant would be related to the combined mobility of charges according to $k_r = e(\mu_{n_1} + \mu_{n_2})/\varepsilon_0\varepsilon_r$. Taking $\mu_{n_1} + \mu_{n_2}$ = 190

DOI: 10.1021/acs.jpcc.8b09665
J. Phys. Chem. C 2019, 123, 841−847

$cm^2\ V^{-1}\ s^{-1}$, $\varepsilon_r = 28$,[52] the recombination rate for the diffusion-limited k_r is then estimated to be $1.2 \times 10^{-5}\ cm^3\ s^{-1}$, which is almost 3 orders of magnitude higher than the value obtained from the fitting. Therefore, the radiative recombination in Te is concluded to be a reaction-limited process, rather than a diffusion-limited process.

Figure 2c,d show the temperature dependence of trap-assisted SRH rates, as well as rates to trapping of charges into an energetically exponential distribution of trap sites. Incorporation of two pathways for charge decay via trapping is the result of the inability to reproduce our experimental data with either type of processes individually. SRH mostly deals with trap-assisted recombination, implying capture of an electron (or a hole) from the conduction band (or valance band) followed by successive recombination with a hole (or an electron) in the valance band (or conduction band). The associated rate constant $k_{n_1}^{SRH}$ (or $k_{n_2}^{SRH}$) depends upon the total trap density N_t, and capture coefficients c_n (or c_p) according to the relation $k_{n_{1/2}}^{SRH} = c_{n_{1/2}} N_t$, where $c_{n_{1/2}} = \sigma_{n_{1/2}} \langle \nu_{th} \rangle$. $\sigma_{n_{1/2}}$ is the electron or hole capture cross section and $\langle \nu_{th} \rangle$ is the thermal velocity of the charges, given by $\langle \nu_{th} \rangle = (3k_B T/m^*_{e/h})^{1/2}$.[41] Therefore, the SRH recombination rate increases with temperature, in contrast to our results in Figure 2c, where a decrease with temperature is observed above 300 K. The decrease could be because of filling of trap sites at higher temperatures by thermally generated intrinsic charges. These competing processes could give rise to a trend as can be clearly seen for one of the charges in Figure 2c in blue. For the case of the other type of charges, as shown in Figure 2d, the thermally generated intrinsic charges may not simply fill the traps, thus the rate constant does not decrease at higher temperatures. The stretched exponential parameter T_0 is found to be 500 ± 100 K, corresponding to an energetic width of 43 ± 9 meV. It is also observed that the stretched exponential parts in the eqs 4 and 5 only determine the longer time scale of the conductivity signals in the range of roughly 25−40 ns. The temperature dependence of characteristic trapping rate constant of the charges $k_{n_{1/2}}$, as shown in green in Figure 2c, is not very pronounced for one type of charges but strongly thermally activated for the other type of charges in Figure 2d. This is similar to the trends observed for trapping of charges in selenium.[9]

Radiative Yield (RY) of Charges. The radiative yield (RY), by definition, is the ratio of the number of photons emitted from the sample and the net number of electrons and holes annihilated radiatively or nonradiatively equaling the generated charge carrier number. The ratio for the instantaneous radiative yield (RY(t)) is given by

$$\mathrm{RY}(t) = (2k_r[n_1(t)n_2(t) - n_i^2])/\left(2\frac{k_{n_1}^{SRH}k_{n_2}^{SRH}[n_1(t)n_2(t) - n_i^2]}{k_{n_1}^{SRH}n_1(t) + k_{n_2}^{SRH}n_2(t)} + \frac{\beta_{n_1}(k_{n_1}t)^{\beta_{n_1}}}{t} + \frac{\beta_{n_2}(k_{n_2}t)^{\beta_{n_2}}}{t} + 2k_r[n_1(t)n_2(t) - n_i^2]\right) \quad (6)$$

with $n(t) = (n_i + \Delta n(t))$. Integrating the numerator and denominator over time yields an estimate for the total (time-integrated) radiative yield (RY), as discussed later. From the theoretical analysis, the 5 ns pulse (peak value in Figure 1a) yields excess densities of electrons and holes equal to density of $(3.7 \pm 0.5) \times 10^{15}\ cm^{-3}$. To compare the significance of decay, namely, radiative recombination, SRH recombination, and stretched-exponential decay, the instantaneous radiative yield expression can be further rewritten, taking the densities of electrons and holes to be equal, as they fall in the aforementioned uncertainty. This simplification enables direct comparison of the processes in the same units. In such a case, the second-order radiative decay rate can be simplified into $k_r[\Delta n(t) + 2n_i]\Delta n(t)$, corresponding to a pseudo-first-order decay with rate $k_r[\Delta n(t) + 2n_i]$. At room temperature, the obtained value for k_r is $(1.1 \pm 0.1) \times 10^{-8}\ cm^3\ s^{-1}$, which yields a value for $k_{1,pseudo}(t = 5\ ns) = k_r\ [\Delta n(t = 5\ ns) + 2n_i] = (5.8 \pm 0.2) \times 10^7\ s^{-1}$, whereas for long-time scale, the value is $k_{1,pseudo}(t \to \infty) = 2k_r n_i = (1.78 \pm 0.04) \times 10^7\ s^{-1}$. Additionally, the room-temperature SRH recombination rate and the characteristic decay rate by stretched-exponential decay are $(7.8 \pm 0.47) \times 10^5$ and $(1.0 \pm 0.5) \times 10^5\ s^{-1}$, respectively, and hence considerably lower than the number above. Using the values for the decay rate constants, Δn (t = 5 ns) and eq 6, the obtained value for the instantaneous RY (t = 5 ns) is ca. 0.98 (or 98%), which decreases to ca. 0.92 (or 92%) for long-time scale (~40 ns), where most of the pulse-generated charges have decayed.

The total RY is obtained by integrating the numerator and denominator, as shown in the following equation

$$\mathrm{RY} = \left(\int_{t_{pulse}}^{\infty} 2k_r[2n_i + \Delta n(t)]dt\right) \Big/ \left(\int_{t_{pulse}}^{\infty} \left[2\frac{[2n_i + \Delta n(t)]}{(\tau_{n_1}^{SRH} + \tau_{n_2}^{SRH})[n_i + \Delta n(t)]} + 2k_r[2n_i + \Delta n(t)] + \frac{\beta_{n_1}(k_{n_1}t)^{\beta_{n_1}}}{t} + \frac{\beta_{n_2}(k_{n_2}t)^{\beta_{n_2}}}{t}\right]dt\right) \quad (7)$$

In the above equation, $\tau_{n_1}^{SRH}$ and $\tau_{n_2}^{SRH}$ are inverse of the corresponding rates $k_{n_1}^{SRH}$ and $k_{n_2}^{SRH}$.

Equation 7 yields a total RY of 0.98 (or 98%). This result indicates a predominant strong radiative recombination in van der Waals bound chains of Te.

For excess densities of electrons and holes on the order of $10^{15}\ cm^{-3}$, the RY yield is much higher than that for a similar band gap material such as black phosphorus,[25] where a comparable RY can be achieved only at an excess density of $10^{19}\ cm^{-3}$. The high RY at a density of $10^{15}\ cm^{-3}$ together with an appreciably high carrier mobility makes Te a material of high potential in efficient infrared light-emitting diodes or laser diodes.[53] Note that a high current is needed in laser diodes to achieve population inversion. On the other hand, it is suitable for very efficient infrared photodetectors with a high bandwidth and a low Johnson noise at high frequency due to appreciably high carrier mobility, as, e.g., in a photoresistor, the noise (voltage) amplitude is proportional to the square root of the inverse mobility via $u_{noise} \approx \sqrt{4k_B TR} = 2L\sqrt{k_B T/e(n_1\mu_{n_1} + n_2\mu_{n_2})}$, with the detector resistance R of a photodetector of length L.[26] At low (modulation) frequencies and/or low temperatures, $1/f$ noise limits the detector performance, resulting in a noise current $I_{noise} = \sqrt{\mathrm{QY}P_S/2h\nu\Delta f}$,[26] with P_S the infrared signal power, Δf the bandwidth, and $h\nu$ the photon energy. From the last equation, it is apparent that a high quantum yield (QY), as measured in Te, is desirable to obtain a high S/N ratio because the signal is proportional to the QY and hence $\mathrm{S/N} \propto \sqrt{\mathrm{QY}}$.

DOI: 10.1021/acs.jpcc.8b09665
J. Phys. Chem. C 2019, 123, 841−847

Hence, Te is an interesting material for applications due to high quantum yield and appreciably high mobility.

CONCLUSIONS

The mobility of charges in Te is thermally deactivated with a room temperature value of 190 ± 20 cm^2 V^{-1} s^{-1}. Charges decay with near unity quantum yield via radiative recombination. Te, being a quasi-one-dimensional van der Waals material, has a potential for in-depth studies of interesting optoelectronic properties with isolated atomic chains. Such chains can in principle be obtained by liquid exfoliation, which offers possibilities for large-scale production. Furthermore, the appreciably high mobility and near-unity radiative yield open the potential for applications in nanoelectronics as efficient far infrared detectors with high bandwidth or lasers with high efficiency. Further, far-infrared imaging applications replacing microbolometers may be of interest.

AUTHOR INFORMATION

Corresponding Authors

*E-mail: p.bhaskar@tudelft.nl (P.B.).
*E-mail: l.d.a.siebbeles@tudelft.nl (L.D.A.S.).

ORCID

Prashant Bhaskar: 0000-0002-5805-9756
Alexander W. Achtstein: 0000-0001-8343-408X
Laurens D. A. Siebbeles: 0000-0002-4812-7495

Present Address

†Technische Universität Berlin, Institut für Optik und Atomare Physik, Straße des 17. Juni 135, D-10623 Berlin, Germany (A.W.A.).

Notes

The authors declare no competing financial interest.

ACKNOWLEDGMENTS

P.B. and L.D.A.S. thank The Netherlands Organisation for Scientific Research (NWO) for financial support. A.W.A. acknowledges the funding by DFG projects AC290/1-1 and AC290/2-1.

REFERENCES

(1) Zhang, W.; Qixing, W.; Yu, C.; Zhuo, W.; Andrew, T. S. W. Van Der Waals Stacked 2d Layered Materials for Optoelectronics. *2D Mater.* **2016**, *3*, No. 022001.
(2) Ajayan, P.; Kim, P.; Banerjee, K. Two-Dimensional Van Der Waals Materials. *Phys. Today* **2016**, *69*, 38−44.
(3) Lin, Z.; Amber, M.; Natalie, B.; Shruti, S.; Kehao, Z.; Yifan, S.; Xufan, L.; Nicholas, J. B.; Hongtao, Y.; Susan, K. F.-S.; Alexey, C.; Hui, Z.; Stephen, M.; Aaron, M. L.; Kai, X.; Brian, J. L.; Marija, D.; James, C. M. H.; Jiwoong, P.; Manish, C.; Raymond, E. S.; Ali, J.; Mark, C. H.; Joshua, R.; Mauricio, T. 2d Materials Advances: From Large Scale Synthesis and Controlled Heterostructures to Improved Characterization Techniques, Defects and Applications. *2D Mater.* **2016**, *3*, No. 042001.
(4) Zhou, X.; Zhang, Q.; Gan, L.; Li, H.; Xiong, J.; Zhai, T. Booming Development of Group Iv−Vi Semiconductors: Fresh Blood of 2d Family. *Adv. Sci.* **2016**, *3*, No. 1600177.
(5) Mak, K. F.; Shan, J. Photonics and Optoelectronics of 2d Semiconductor Transition Metal Dichalcogenides. *Nat. Photonics* **2016**, *10*, 216.
(6) Zhang, C.; Cheng, G.; Yifan, N.; Kyung-Ah, M.; Chaoping, L.; Young Jun, O.; Hengji, Z.; Weihua, W.; Suklyun, H.; Luigi, C.; Robert, M. W.; Kyeongjae, C. Systematic Study of Electronic Structure and Band Alignment of Monolayer Transition Metal Dichalcogenides in Van Der Waals Heterostructures. *2D Mater.* **2017**, *4*, No. 015026.
(7) Yu, X.; Sivula, K. Layered 2d Semiconducting Transition Metal Dichalcogenides for Solar Energy Conversion. *Curr. Opin. Electrochem.* **2017**, *2*, 97−103.
(8) Choi, W.; Choudhary, N.; Han, G. H.; Park, J.; Akinwande, D.; Lee, Y. H. Recent Development of Two-Dimensional Transition Metal Dichalcogenides and Their Applications. *Mater. Today* **2017**, *20*, 116−130.
(9) Bhaskar, P.; Achtstein, A. W.; Diedenhofen, S. L.; Siebbeles, L. D. A. Mobility and Decay Dynamics of Charge Carriers in One-Dimensional Selenium Van Der Waals Solid. *J. Phys. Chem. C* **2017**, *121*, 18917−18921.
(10) Churchill, H. O. H.; Salamo, G. J.; Yu, S.-Q.; Hironaka, T.; Hu, X.; Stacy, J.; Shih, I. Toward Single Atom Chains with Exfoliated Tellurium. *Nanoscale Res. Lett.* **2017**, *12*, 488.
(11) Liu, Y.; Wu, W.; Goddard, W. A. Tellurium: Fast Electrical and Atomic Transport Along the Weak Interaction Direction. *J. Am. Chem. Soc.* **2018**, *140*, 550−553.
(12) Caldwell, R. S.; Fan, H. Y. Optical Properties of Tellurium and Selenium. *Phys. Rev.* **1959**, *114*, 664−675.
(13) Stuke, J. Recent Progress in the Physics of Selenium and Tellurium. In *The Physics of Selenium and Tellurium*; Pergamon, 1969; pp 3−20.
(14) Hulin, M. Electron Band Structure of Tellurium. *J. Phys. Chem. Solids* **1966**, *27*, 441−449.
(15) Lutz, M.; Stolze, H.; Grosse, P. The Masses of Free Holes and Electrons in Tellurium. *Phys. Status Solidi B* **1974**, *62*, 665−675.
(16) Treusch, J.; Sandrock, R. Energy Band Structures of Selenium and Tellurium (Kohn-Rostoker Method). *Phys. Status Solidi B* **1966**, *16*, 487−497.
(17) Tutihasi, S.; Roberts, G. G.; Keezer, R. C.; Drews, R. E. Optical Properties of Tellurium in the Fundamental Absorption Region. *Phys. Rev.* **1969**, *177*, 1143−1150.
(18) Bondar, V. M.; Radchenko, V. S.; Solonchuk, L. S. Conductivity of Warm Holes in Tellurium. *Phys. Status Solidi B* **1978**, *87*, K97−K100.
(19) Bohmeyer, W.; Hoerstel, W. Hall Effect in P-Tellurium at High Electric Fields. *Phys. Status Solidi A* **1977**, *41*, K27−K30.
(20) Hoerstel, W.; Kusnick, D.; Spitzer, M. High-Field Transport and Low-Field Mobility in Tellurium Single Crystals. *Phys. Status Solidi B* **1973**, *60*, 213−221.
(21) Nimtz, G.; Seeger, K. Current Controlled Negative Differential Resistivity of P-Type Tellurium. *Appl. Phys. Lett.* **1969**, *14*, 19−21.
(22) Peng, H.; Kioussis, N.; Snyder, G. J. Elemental Tellurium as a Chiral P-Type Thermoelectric Material. *Phys. Rev. B* **2014**, *89*, No. 195206.
(23) Lin, S.; Li, W.; Chen, Z.; Shen, J.; Ge, B.; Pei, Y. Tellurium as a High-Performance Elemental Thermoelectric. *Nat. Commun.* **2016**, *7*, No. 10287.
(24) Zhou, G.; Addou, R.; Wang, Q.; Honari, S.; Cormier, C. R.; Cheng, L.; Yue, R.; Smyth, C. M.; Laturia, A.; Kim, J.; Vandenberghe, W. G.; Kim, M. J.; Wallace, R. M.; Hinkle, C. L. High-Mobility Helical Tellurium Field-Effect Transistors Enabled by Transfer-Free, Low-Temperature Direct Growth. *Adv. Mater.* **2018**, *30*, No. 1803109.
(25) Bhaskar, P.; Achtstein, A. W.; Vermeulen, M. J. W.; Siebbeles, L. D. A. Radiatively Dominated Charge Carrier Recombination in Black Phosphorus. *J. Phys. Chem. C* **2016**, *120*, 13836−13842.
(26) Boyd, R. W. *Radiometry and the Detection of Optical Radiation*; Wiley, 1983.
(27) Bethe, H.; Heitler, W. On the Stopping of Fast Particles and on the Creation of Positive Electrons. *Proc. R. Soc. A* **1934**, *146*, 83−112.
(28) Bethe, H.; Hund, F.; Mott, N. F.; Pauli, W.; Rubinowicz, A.; Wentzel, G.; Smekal, A. *Quantentheorie*; Springer-Verlag: Berlin, 1933.
(29) Report 16. Linear Energy Transfer. *J. ICRU* **1970**, *os9*, 1−51.
(30) Mozumder, A. Interaction of Radiation with Matter: Energy Transfer from Fast Charged Particles. In *Fundamentals of Radiation Chemistry*; Mozumder, A., Ed.; Academic Press: San Diego, 1999; Chapter 2, pp 5−39.

DOI: 10.1021/acs.jpcc.8b09665
J. Phys. Chem. C 2019, 123, 841−847

(31) Turner, J. E. *Atoms, Radiation, and Radiation Protection*; Wiley-VCH Verlag GmbH & Co. KGaA, 2007.
(32) Warman, J. M.; de Haas, M. P.; Wentinck, H. M. The Study of Radiation Induced Conductivity Changes in Microheterogeneous Materials Using Microwaves. *Int. J. Radiat. Appl. Instrum., Part C* **1989**, *34*, 581−586.
(33) Coelho, R. *Physics of Dielectrics for the Engineer*; Elsevier Scientific: Amsterdam; New York, 1979.
(34) Hoofman, R. J. O. M.; Siebbeles, L. D. A.; de Haas, M. P.; Hummel, A.; Bloor, D. Anisotropy of the Charge-Carrier Mobility in Polydiacetylene Crystals. *J. Chem. Phys.* **1998**, *109*, 1885−1893.
(35) Grozema, F. C.; Hoofman, R. J. O. M.; Candeias, L. P.; de Haas, M. P.; Warman, J. M.; Siebbeles, L. D. A. The Formation and Recombination Kinetics of Positively Charged Poly(Phenylene Vinylene) Chains in Pulse-Irradiated Dilute Solutions. *J. Phys. Chem. A* **2003**, *107*, 5976−5986.
(36) Alig, R. C.; Bloom, S.; Struck, C. W. Scattering by Ionization and Phonon Emission in Semiconductors. *Phys. Rev. B* **1980**, *22*, 5565−5582.
(37) Infelta, P. P.; de Haas, M. P.; Warman, J. M. The Study of the Transient Conductivity of Pulse Irradiated Dielectric Liquids on a Nanosecond Timescale Using Microwaves. *Radiat. Phys. Chem.* **1977**, *10*, 353−365.
(38) Piprek, J. Carrier Transport. In *Semiconductor Optoelectronic Devices*; Academic Press: Boston, 2003; Chapter 3, pp 49−82.
(39) Piprek, J. Introduction to Semiconductors. In *Semiconductor Optoelectronic Devices*; Academic Press: Boston, 2003; Chapter 1, pp 3−11.
(40) Piprek, J.; Römer, F.; Witzigmann, B. On the Uncertainty of the Auger Recombination Coefficient Extracted from Ingan/Gan Light-Emitting Diode Efficiency Droop Measurements. *Appl. Phys. Lett.* **2015**, *106*, No. 101101.
(41) Li, S. S. *Semiconductor Physical Electronics*, 2nd ed.; Springer: New York, 2006.
(42) Berberan-Santos, M. N.; Bodunov, E. N.; Valeur, B. Mathematical Functions for the Analysis of Luminescence Decays with Underlying Distributions 1. Kohlrausch Decay Function (Stretched Exponential). *Chem. Phys.* **2005**, *315*, 171−182.
(43) Dicker, G.; de Haas, M. P.; de Leeuw, D. M.; Siebbeles, L. D. A. Origin of the Stretched-Exponential Hole Relaxation in Regioregular Poly(3-Hexylthiophene). *Chem. Phys. Lett.* **2005**, *402*, 370−374.
(44) Dicker, G.; de Haas, M. P.; Warman, J. M.; de Leeuw, D. M.; Siebbeles, L. D. A. The Disperse Charge-Carrier Kinetics in Regioregular Poly(3-Hexylthiophene). *J. Phys. Chem. B* **2004**, *108*, 17818−17824.
(45) Pfister, G.; Scher, H. Dispersive (Non-Gaussian) Transient Transport in Disordered Solids. *Adv. Phys.* **1978**, *27*, 747−798.
(46) Silver, M.; Schoenherr, G.; Baessler, H. Dispersive Hopping Transport from an Exponential Energy Distribution of Sites. *Phys. Rev. Lett.* **1982**, *48*, 352−355.
(47) Schnörer, H.; Haarer, D.; Blumen, A. Crossover from Dispersive to Nondispersive Transport in a Trap-Controlled Hopping Model. *Phys. Rev. B* **1988**, *38*, 8097−8101.
(48) Gfroerer, T. H.; Priestley, L. P.; Fairley, M. F.; Wanlass, M. W. Temperature Dependence of Nonradiative Recombination in Low-Band Gap Inxga1-Xas/Inasyp1-Y Double Heterostructures Grown on Inp Substrates. *J. Appl. Phys.* **2003**, *94*, 1738−1743.
(49) Mort, J. Transient Photoconductivity in Trigonal Selenium Single Crystals. *J. Appl. Phys.* **1968**, *39*, 3543−3549.
(50) Wang, Y.; Qiu, G.; Wang, R.; Huang, S.; Wang, Q.; Liu, Y.; Du, Y.; Goddard, W. A.; Kim, M. J.; Xu, X.; Ye, P. D.; Wu, W. Field-Effect Transistors Made from Solution-Grown Two-Dimensional Tellurene. *Nat. Electron.* **2018**, *1*, 228−236.
(51) Cheng, L.; Liu, Y. What Limits the Intrinsic Mobility of Electrons and Holes in Two Dimensional Metal Dichalcogenides? *J. Am. Chem. Soc.* **2018**, DOI: 10.1021/jacs.8b07871.
(52) Young, K. F.; Frederiske, H. P. R. Compilation of the Static Dielectric Constant of Inorganic Solids. *J. Phys. Chem. Ref. Data* **1973**, *2*, 313−409.
(53) Sorokina, I. T.; Vodopyanov, K. L. *Solid-State Mid-Infrared Laser Sources*; Springer Science & Business Media, 2003; Vol. *89*.

DOI: 10.1021/acs.jpcc.8b09665
J. Phys. Chem. C 2019, 123, 841−847